Environmental Pollution 234 (2018) 794–803

Contents lists available at ScienceDirect

Environmental Pollution

journal homepage: www.elsevier.com/locate/envpol

Spatiotemporal characterization and mapping of $PM_{2.5}$ concentrations in southern Jiangsu Province, China☆

Yong Yang [a, b], George Christakos [c, d, *], Xue Yang [a, b], Junyu He [c, d]

[a] College of Resources & Environment, Huazhong Agricultural University, Wuhan, China
[b] Key Laboratory of Arable Land Conservation (Middle & Lower Reaches of Yangtse River), Ministry of Agriculture, China
[c] Institute of Island & Coastal Ecosystems, Ocean College, Zhejiang University, Zhoushan, China
[d] Department of Geography, San Diego State University, San Diego, CA, USA

ARTICLE INFO

Article history:
Received 12 September 2017
Received in revised form
23 November 2017
Accepted 24 November 2017

Keywords:
Spatiotemporal variation
$PM_{2.5}$
Pollution
China
Kriging

ABSTRACT

As a result of rapid industrialization and urbanization, China is experiencing severe air pollution problems. Understanding the spatiotemporal variation and trends of air pollution is a key element of an improved understanding of the underlying physical mechanisms and the implementation of the most effective risk assessment and environmental policy in the region. The motivation behind the present work is that the study region of southern Jiangsu province of China is one of the most populated and developed regions in China. The daily concentrations of particulate matter with particle diameter smaller than 2.5 μm ($PM_{2.5}$) in southern Jiangsu province obtained during the year 2014 were used to derive the variogram model that provided a quantitative characterization of the spatiotemporal (ST) variation of $PM_{2.5}$ concentrations in the study region. A spatiotemporal ordinary kriging (STOK) technique was subsequently employed to generate informative maps of the ST pollutant distribution in southern Jiangsu province. The results generated by STOK showed that during 2014 about 29.3% of the area was $PM_{2.5}$ polluted (at various severity levels, according to the criteria established by the Chinese government), and that the number of days characterized as polluted varied from 59 to 164 at different parts of the study region. Nanjing, the capital of Jiangsu province, was the place with the highest $PM_{2.5}$ pollution (including 3 days of serious pollution). The $PM_{2.5}$ pollution exhibited a decreasing spatial trend from the western to the eastern part of southern Jiangsu. A similar temporal $PM_{2.5}$ pattern was found from the western to the eastern part of southern Jiangsu, which was characterized by 4 peaks and 3 troughs linked to different meteorological conditions and human factors.

1. Introduction

In recent years, as a result of industrialization and urbanization in China, atmospheric particulate matter (PM) pollution has become a serious environmental problem (Hu et al., 2014). Accordingly, environmental research in China is increasingly focusing on PM pollution assessment, including its spatial patterns, source apportionment, migration and transformation, and subsequent control measures (Zhao et al., 2014; Zhang et al., 2017). In this setting, the accurate characterization and mapping of the spatiotemporal (ST) pollutant distribution play a fundamental role. Since 2013, China's government has begun to release information about major ambient pollutants, including particulate matter with particle diameter smaller than 2.5 μm ($PM_{2.5}$), particulate matter with particle diameter smaller than 10 μm (PM_{10}), sulfur dioxide (SO_2), carbon monoxide (CO), and nitrogen dioxide (NO_2) at major cities and at an hourly rate. These data provide the basis for the modeling and evaluation of regional air pollution.

However, most of the PM correlation studies in China did not involve any rigorous ST modeling of atmospheric pollution, but they rather focused on a purely spatial representation of the situation, followed by an *ad hoc* quantitative analysis of the situation based on the results obtained during multiple time periods (Fang et al., 2016; Chen et al., 2016; Wang and Fang, 2016). Methodologically, this is like one is trying to fit the (spatiotemporal) reality to a (spatial) model, rather than fit a (spatiotemporal) model to the (spatiotemporal) reality. This is certainly paradoxical, given that

☆ This paper has been recommended for acceptance by Dr. Hageman Kimberly Jill.

* Corresponding author. Hai Ke Building 421, No.1 Zheda Road, Lincheng Street, Dinghai District, Zhoushan, Zhejiang, 316021, China.
E-mail address: gchristakos@zju.edu.cn (G. Christakos).

https://doi.org/10.1016/j.envpol.2017.11.077
0269-7491/

international studies have shown that air pollution characterization and mapping based on composite ST modeling offer a more accurate representation of PM distribution and allow a better understanding of the PM variation mechanisms than purely spatial data analysis (Christakos and Serre, 2000; Christakos et al., 2001; Snepvangers et al., 2003; Pang et al., 2009; Yang et al., 2014; Calculli et al., 2015; Fassò et al., 2016; Datta et al., 2016). Moreover, there exist physically significant cross space-time dependencies (visualized as diagonal correlations) in the $PM_{2.5}$ distribution. For example, depending on the meteorological conditions (wind direction, atmospheric pressure etc.), the high $PM_{2.5}$ concentration observed at location A today may affect the concentration at a different location B tomorrow to a larger degree than the $PM_{2.5}$ concentration at location B today affects the concentration at the same location B tomorrow. In the present study, in particular, the limited monitoring stations offer a relative sparse spatial coverage of the study region. Thus, the prediction (estimation) accuracy obtained from a spatial interpolation technique (e.g., spatial kriging) will be worse than that of spatiotemporal interpolation technique. Also, if the spatial kriging is used to predict spatial $PM_{2.5}$ concentrations in the study region separately for each time (e.g., day), it would be necessary to fit a separate spatial variogram model and run a spatial kriging algorithm for each individual day (a total of 365 models with the corresponding algorithms), in which case the workload would be very heavy and the space-time separable approach rather unrealistic. Therefore, ST analysis models are more adequate to explore the implicit information contained in the ST data and to help us reveal the mechanism of the ST variation for geographical attributes.

In view of the above considerations, the present work has three main goals: (a) to compute the empirical ST variograms and fit the theoretical variogram models that describe adequately the physical space-time variations of daily $PM_{2.5}$ concentrations in southern Jiangsu Province (China) during the year 2014; (b) to generate maps of the spatiotemporal $PM_{2.5}$ distribution using the spatiotemporal ordinary kriging technique (STOK, Christakos, 1992); and (c) based on the findings of (a) and (b), to provide a quantitative characterization of $PM_{2.5}$ pollution in the study region for risk assessment and population health management purposes.

2. Material and methods

2.1. Study area and data

The focus of this study is southern Jiangsu province, which is one of the most populated and developed area in China (Wang et al., 2016; Shen et al., 2014). Therefore, it is quite important to accurately assess the ST variation of the $PM_{2.5}$ concentrations in southern Jiangsu. The data used in this study were obtained at 53 monitoring sites at 5 cities of the southern Jiangsu region (Nanjing, Zhenjiang, Changzhou, Wuxi, and Suzhou, with a total of 22470 km^2) during the period January 1—December 31, 2014 (Fig. 1, top). The data used in the study were collected from the website http://106.37.208.233:20035/. The Ministry of Environmental Protection of the People's Republic of China (MEPPRC) releases real-time hourly concentrations of major ambient pollutant concentrations in this website. The ambient $PM_{2.5}$ concentrations were measured in-situ according to the Chinese Environmental Protection Standard HJ655-2013 (NHFPCC, 2013), and the daily $PM_{2.5}$ concentration were derived at each site by averaging the hourly data. The descriptive statistics and the histogram of the $PM_{2.5}$ concentration data used in this study are also shown in Fig. 1 (bottom). The mean $PM_{2.5}$ concentration was 65.63 $\mu g/m^3$, and the coefficient of variation (CV) was 0.57, indicating a medium level variability of the monitored $PM_{2.5}$ data (note that $0.1 < CV < 1$).

The daily $PM_{2.5}$ concentrations averaged over all monitoring sites available in the study region during the year 2014 are plotted in Fig. 2. This is a time series constructed on the basis of the original (raw) $PM_{2.5}$ data, which exhibits a seasonal pattern with elevated concentrations during spring and winter due to seasonal fluctuations of both the emissions and meteorological conditions (for a relevant discussion, see Hu et al., 2014). We notice that the stations were sorted/labeled according to their S_2 values (Fig. 1 top), and for every group of 5 stations one was sequentially selected as the validation station, so that in the end a total number of 3611 samples from 10 stations (almost 20% of all monitoring stations) served as the validation dataset.

2.2. Spatiotemporal ordinary Kriging (STOK)

Air pollutants, such as $PM_{2.5}$ or PM_{10} concentrations in the atmosphere, are physical attributes that develop simultaneously in space and time under conditions of uncertainty. The simultaneous space and time variation of $PM_{2.5}$ concentrations in southern Jiangsu is best represented mathematically in terms of the spatiotemporal random field model (S/TRF)

$$PM_{2.5}(\boldsymbol{p}) = \{PM_{2.5} : \boldsymbol{p} = (\boldsymbol{s}, t), \boldsymbol{s} = (s_1, s_2) \in S, t \in T\},$$

which is defined on a geographical domain $S \in R^2$ and a time period $T \in R^1$ in a way that distinguishes between the physically different arguments of space and time. In-situ uncertainty is represented in the S/TRF model by a collection of possible ST $PM_{2.5}$ realizations, where the likelihood of each one of these realizations occurring is computed by the $PM_{2.5}$ probability law. The ST distance between the points $\boldsymbol{p}_i$ and $\boldsymbol{p}_j$ separated by the space distance $\boldsymbol{h}_{ij}$ and the time difference τ_{ij} is denoted by the vector

$$\boldsymbol{p}_j - \boldsymbol{p}_i = \Delta \boldsymbol{p}_{ij} = (\boldsymbol{h}_{ij}, \tau_{ij}),$$

$i, j = 1, 2, \ldots, n$ (for a detailed technical presentation of the S/TRF model, see Christakos, 1992, 2017).

The ST pollutant variation (which is due to physical processes and mechanisms) is quantitatively expressed in terms of the correlation between $PM_{2.5}$ concentrations at any pair of points $\boldsymbol{p}_i$ and $\boldsymbol{p}_j$. This correlation is represented by the variogram $\gamma_{PM_{2.5}}(\boldsymbol{h}_{ij}, \tau_{ij})$, which is a function of the space lag $\boldsymbol{h}_{ij}$ and the time separation τ_{ij} between $\boldsymbol{p}_i$ and $\boldsymbol{p}_j$. Two types of variogram functions are considered in the S/TRF modeling setting: (a) the empirical (experimental) variogram that is computed only between the $PM_{2.5}$ sampling points (say N points), and (b) the theoretical variogram (fitted to the empirical variogram) that provides $PM_{2.5}$ correlation values between any pair of points on the ST mapping grid (say $n > N$ grid points). In particular, the empirical ST variogram was calculated in this study based on the $PM_{2.5}$ data available at points $\boldsymbol{p}_i$ ($i = 1, 2, \ldots, N$) using the formula

$$\widehat{\gamma}_{PM_{2.5}}(h_S, h_T) = \frac{1}{2N(h_S, h_T)} \sum_{i=1}^{N(h_S, h_T)} [PM_{2.5}(s_i, t_i) - PM_{2.5}(s_i + h_S, t_i + h_T)]^2 \quad (1)$$

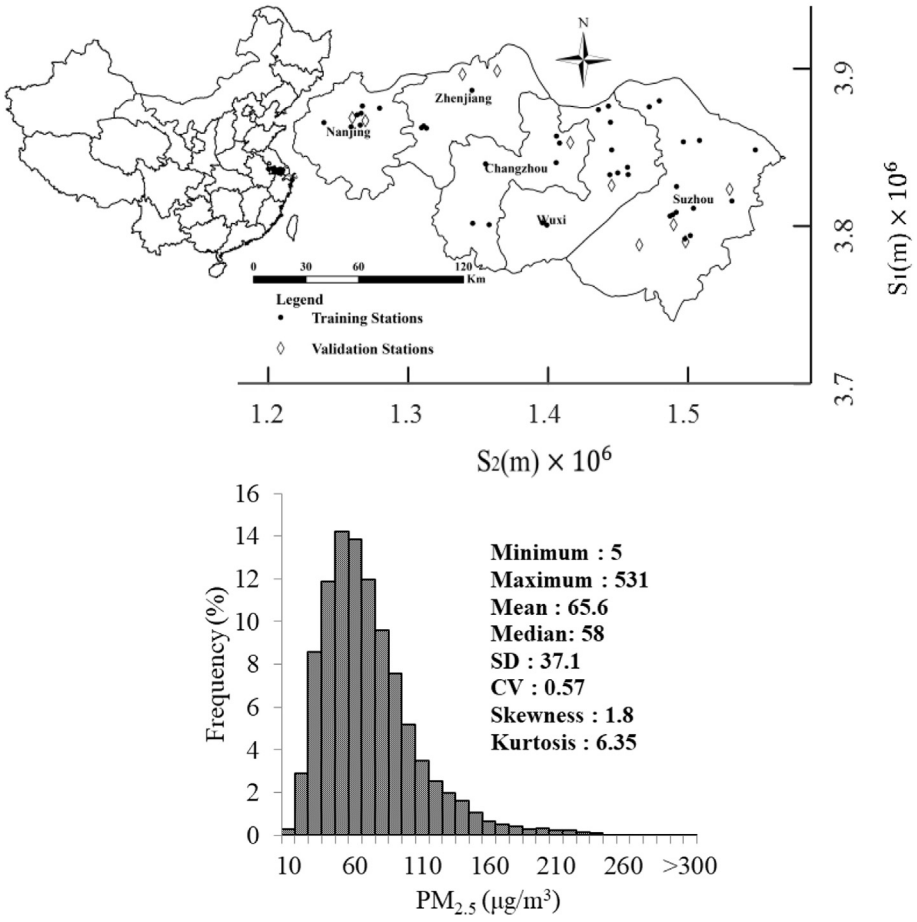

Fig. 1. (Top) Geographical location of the study area, and spatial locations of the monitoring sites (Geographic coordinate system: GCS Beijing 1954; Projected coordinated system: Asia lambert conformal conic). (Bottom) Summary statistics and histogram of the $PM_{2.5}$ concentrations ($\mu g/m^3$) of all the collected data in southern Jiangsu during 2014 (SD, standard deviation; CV, coefficient of variation).

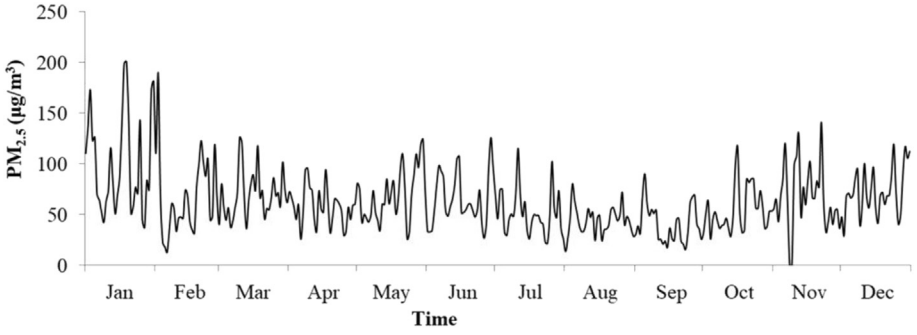

Fig. 2. Daily variation of monitored $PM_{2.5}$ mean concentrations ($\mu g/m^3$) in southern Jiangsu during 2014.

where h_S and h_T are the spatial and temporal sampling lags, and $N(h_S, h_T)$ is the number of pairs of sampling points separated by h_S and h_T. Since the empirical variogram is calculated only for the sampling lags h_S and h_T, the STOK technique requires knowledge of the variogram values at any ST lags $h_{ij} \in S$, $\tau_{ij} \in T$ $(i, j = 1, 2, \ldots, n)$, the next step is to select a suitable theoretical model $\gamma_{PM_{2.5}}(\boldsymbol{h}_{ij}, \tau_{ij})$ to fit to the empirical variogram. There are various theoretical ST variogram models available in the relevant literature, including both separable and non-separable models (Christakos, 1992, 2017; Christakos and Hristopulos, 1998; De Cesare et al., 2001; De Iaco et al., 2003; Gneiting, 2002; Kolovos et al., 2004; Ma, 2008; Porcu et al., 2008).

Based on the selected theoretical variogram model $\gamma_{PM_{2.5}}(\boldsymbol{h}_{ij}, \tau_{ij})$, the $PM_{2.5}$ variations at all ST lags required by the STOK kriging technique were calculated. Then, the STOK equations in matrix form can be expressed as

$$\begin{bmatrix} \gamma_{PM_{2.5}}(\boldsymbol{p}_1,\boldsymbol{p}_1) & \gamma_{PM_{2.5}}(\boldsymbol{p}_1,\boldsymbol{p}_2) & \cdots & \gamma_{PM_{2.5}}(\boldsymbol{p}_1,\boldsymbol{p}_n) & 1 \\ \gamma_{PM_{2.5}}(\boldsymbol{p}_2,\boldsymbol{p}_1) & \gamma_{PM_{2.5}}(\boldsymbol{p}_2,\boldsymbol{p}_2) & \cdots & \gamma_{PM_{2.5}}(\boldsymbol{p}_2,\boldsymbol{p}_n) & 1 \\ \vdots & \vdots & \cdots & \vdots & \vdots \\ \gamma_{PM_{2.5}}(\boldsymbol{p}_n,\boldsymbol{p}_1) & \gamma_{PM_{2.5}}(\boldsymbol{p}_n,\boldsymbol{p}_2) & & \gamma_{PM_{2.5}}(\boldsymbol{p}_n,\boldsymbol{p}_n) & 1 \\ 1 & 1 & \cdots & 1 & 0 \end{bmatrix} \times \begin{bmatrix} \lambda_1 \\ \lambda_2 \\ \vdots \\ \lambda_n \\ \mu \end{bmatrix} = \begin{bmatrix} \gamma_{PM_{2.5}}(\boldsymbol{p}_1,\boldsymbol{p}_0) \\ \gamma_{PM_{2.5}}(\boldsymbol{p}_2,\boldsymbol{p}_0) \\ \vdots \\ \gamma_{PM_{2.5}}(\boldsymbol{p}_n,\boldsymbol{p}_0) \\ 1 \end{bmatrix} \tag{2}$$

where $\boldsymbol{p}_0$ denotes an (unsampled) ST point on a mapping grid where the $PM_{2.5}$ concentration needs to be estimated, $\boldsymbol{p}_i$ $(i = 1, 2, \ldots, n)$ are neighboring sampling points,

$$\gamma_{PM_{2.5}}\left(\boldsymbol{p}_i, \boldsymbol{p}_j\right) = \gamma_{PM_{2.5}}(\boldsymbol{h}_{ij}, \tau_{ij})$$

denotes the variogram value expressing quantitatively the correlation between $PM_{2.5}$ concentrations at ST points $\boldsymbol{p}_i$ and $\boldsymbol{p}_j$ at space lag $\boldsymbol{h}_{ij}$ and time separation τ_{ij}, and λ_i, μ are unknown coefficients to be calculated from the solution of the STOK system of Eq (2). After the λ_i $(i = 1, 2, \ldots, n)$, μ have been calculated, the STOK-predicted (estimated) $PM_{2.5}$ value and the associated STOK prediction (estimation) error variance at each $\boldsymbol{p}_0$ of the mapping grid can be obtained, respectively, as follows,

$$PM^{*}_{2.5}(\boldsymbol{p}_0) = \sum_{i=1}^{n} \lambda_i PM_{2.5}(\boldsymbol{p}_i) \tag{3}$$

$$\sigma^2_{PM_{2.5}}(p_0) = \begin{bmatrix} \gamma_{PM_{2.5}}(p_1,p_0) \\ \gamma_{PM_{2.5}}(p_1,p_0) \\ \vdots \\ \gamma_{PM_{2.5}}(p_1,p_0) \\ 1 \end{bmatrix}^{T} \times \begin{bmatrix} \lambda_1 \\ \lambda_2 \\ \vdots \\ \lambda_n \\ \mu \end{bmatrix} = \sum_{i=1}^{n} \lambda_i \gamma_{PM_{2.5}}(p_i,p_0) + \mu \tag{4}$$

That is, both a prediction of the $PM_{2.5}$ concentration, Eq (3), and a measure of the associated accuracy of this prediction, Eq (4), are derived at each (unsampled) point $\boldsymbol{p}_0$ of the mapping grid. Notice that $\sigma^2_{PM_{2.5}}(\boldsymbol{p}_0)$ is independent of the $PM_{2.5}$ data, which makes it a valuable tool of sampling network design. In the present study, STOK was performed with the following specifications:

Grid nodes: 85 (*rows*) × 150 (*column*) × 365 (*days*).
Spatiotemporal cell size: 2000 (*m*) × 2000 (*m*) × 1 (*day*).
Time period: January 1st to December 31st, 2014.

Subsequently, the STOK results were cropped by boundaries of the study region (see Fig. 1 top).

2.3. ST variation analysis

A ST variation analysis of the $PM_{2.5}$ concentration prediction maps generated by STOK was subsequently carried out that improved our understanding of the spatial and temporal patterns of $PM_{2.5}$ concentration.

2.3.1. Spatial distribution of the mean and coefficient of variation (CV)

The $PM_{2.5}$ mean and CV were used to evaluate the concentricity and variability of $PM_{2.5}$ concentrations in the study region. Specifically, two maps of the spatial distribution of the temporal pollutant mean were obtained, and the average $PM_{2.5}$ concentrations at each spatial location $\boldsymbol{s}$ within the region were defined as

$$\overline{PM_{2.5}}(\boldsymbol{s}) = \frac{1}{365} \sum_{i=1}^{365} PM_{2.5}(\boldsymbol{s}, t_i) \tag{5}$$

$$\overline{PM^{\geq}_{2.5}}(\boldsymbol{s}) = \frac{1}{M} \sum_{i=1}^{M} PM^{\geq}_{2.5}(\boldsymbol{s}, t_i) \tag{6}$$

where $PM^{\geq}_{2.5}(\boldsymbol{s}, t_i)$ means that the $PM_{2.5}$ concentration at $(\boldsymbol{s}, t_i)$ is greater or equal to a given threshold $PM^{c}_{2.5}$, and M is the number of corresponding days when $PM^{\geq}_{2.5}$ occurs. Otherwise said, $\overline{PM_{2.5}}(\boldsymbol{s})$ is the annual $PM_{2.5}$ average concentration at location $\boldsymbol{s}$ and $\overline{PM^{\geq}_{2.5}}(\boldsymbol{s})$ is the mean $PM_{2.5}$ concentration at $\boldsymbol{s}$ only during those days that $PM^{\geq}_{2.5}(\boldsymbol{s}, t_i)$ occurs. Accordingly, two CVs were defined at each location $\boldsymbol{s}$: one is the ratio of the $PM_{2.5}$ standard deviation over the mean $\overline{PM_{2.5}}(\boldsymbol{s})$, and the other is the ratio of the $PM^{\geq}_{2.5}(\boldsymbol{s}, t_i)$ standard deviation over the mean $\overline{PM^{\geq}_{2.5}}(\boldsymbol{s})$.

2.3.2. Spatial distribution of the number of days beyond the given threshold

As shown in Table 1, according to the China National Ambient Air Quality Standard (MEPPRC, 2012), the $PM_{2.5}$ ambient concentration was divided into six intervals corresponding to six levels, the spatial distribution of the number of days during a year that $PM_{2.5}$ concentration exceeded those levels was considered, and the air quality was characterized as shown in Table 1.

2.3.3. Temporal analysis of the $PM_{2.5}$ at different geographic locations

According to the distribution of the monitoring sites at different geographical locations, the spatial pattern of the mean $PM_{2.5}$ concentrations in the study region was characterized by an increasing concentration trend from the east to the west. The average daily $PM_{2.5}$ concentrations at grid nodes with a common horizontal coordinate s_2 and vertical coordinates s^j_1 was calculated by

$$PM^{N_V}_{2.5}(s_2, t_i) = \frac{1}{N_V} \sum_{j=1}^{N_V} PM_{2.5}\left(s^j_1, s_2, t_i\right) \tag{7}$$

$(i = 1, 2, \ldots, 365)$, where N_V is the number of grid nodes with horizontal ordinate s_2 in the study region. Subsequently, the Dynamic Harmonic Regression method (DHR) was employed to model the trend of the original $PM_{2.5}$ time series. The DHR method was developed by Young et al. (1999) to perform frequency domain time series analysis according to the characteristics of the spectrum of the original time series. The DHR model is used to fit three main components in a time series: the trend component of the original values T_t, the inherent seasonal component S_t, and the residual values e_t. In the present study, the trend component T_t was separated from the original $PM_{2.5}$ time series because the temporal analysis of $PM_{2.5}$ concerned one year (2014). The DHR steps at each spatial location were as follows: (1) Based on the characteristics of the original $PM_{2.5}$ time series the main models (e.g. General Random Walker model) were selected to express the entire $PM_{2.5}$ time series during 2014; (2) the model parameters were estimated; (3) using the estimated parameters in step (2) each time series component was computed using the parameters estimated in step 2 above (more technical details about the DHR method can be found in Young et al., 1999 and Jiang et al., 2010). Lastly, we notice that the DHR model was implemented in this study using the

Table 1
Grading standards of $PM_{2.5}$ ambient concentration (MEPPRC, 2012).

Level of air quality	Mean $PM_{2.5}$ value within 24 h ($\mu g/m^3$)	Type of air quality
Level 1	0–35	Excellent
Level 2	35–75	Good
Level 3	75–115	Light pollution
Level 4	115–150	Moderate pollution
Level 5	150–250	Heavy pollution
Level 6	>250	Serious pollution

Captain Toolbox (download from the website: www.es.lancs.ac.uk/cres/captain), which was developed on the MATLAB software platform by Young et al. (2007).

3. Results

3.1. ST variogram

For the original $PM_{2.5}$ concentration data in the southern Jiangsu, the calculated Kolmogorov-Smirnov (K-S) test value was 0.0001 ($P < 0.005$), indicating that the null hypothesis of a normal distribution was rejected for the data used in this study. Accordingly, the original $PM_{2.5}$ data were logarithmically transformed so that they obey a normal distribution (the K-S test value was 4.01, and the summary statistics and histogram of the logarithmically transformed data are shown in Fig. S1). Then, the empirical (experimental) ST variogram of the log-transformed $PM_{2.5}$ concentrations was computed as described earlier (see, discussion of Eq (1)), and the theoretical ST non-separable variogram model (Kolovos et al., 2004)

$$\gamma(h_{ij},\tau_{ij}) = (c_0 + c) - c\left[1 + \frac{1}{w^2}(h_{ij} + \alpha\tau_{ij})^2\right]^{-\frac{\nu}{2}} e^{-\frac{1}{\xi}|h_{ij}+\alpha\tau_{ij}|} \qquad (8)$$

was selected as the best fit to the corresponding empirical variogram, where c_0, c, w, α, ν and ξ are model parameters to be calculated by fitting the model (8) to the empirical variogram (specifically, c_0 is the nugget value, $c_0 + c$ is the sill value, and α is the coefficient corresponding to the spatial and temporal correlation scale; the w, ξ, ν are empirically calculated coefficients that allow flexibility in achieving an optimal fit). In particular, with the help of the "cftool" box of Matlab software it was found that $c_0 = 0.02196(\mu g/m^3)^2$, $c = 0.5063(\mu g/m^3)^2$, w = -1.87e+05(m), $\alpha = 4.941e+05\left(\frac{m}{day}\right)$, $\nu = -2.229$ and ξ = 1.629e+05(m) ($R^2 = 0.912$, RMSE = 0.0333). The results are presented in Fig. 3a.

As is shown in Fig. 3a, the theoretical variogram model (8) closely follows the pattern of the empirical ST variogram (black dots in Fig. 3a), indicating that the fitted model adequately represents the actual ST correlations between the $logPM_{2.5}$ concentration values. By virtue of the S/TRF theory, the asymptotic shape of the variogram (with a maximum value of $c_0 + c = 0.528$, Fig. 3a) implies that the variation of the log-transformed $PM_{2.5}$ data is spatially homogeneous (technically, the mean is constant across space and the variogram depends only on the spatial distance between two locations and not on the individual locations), and temporally stationary (technically, the mean is constant in time and the variogram depends only on the separation time between two points and not on the individual times). We note that when back-transformed the resulting $PM_{2.5}$ maps include the existing space-time trends of the raw data. In the spatial direction, there is a constant and slow increase in the variogram values until a spatial lag of approximately 140 km. We notice the significant increase in the variogram values with increasing spatial distance. As they approach the 140 Km distance the variogram values fluctuate around a certain constant value. This is true at zero separation time ($\tau = 0$), but also at longer separation times $\tau > 0$. On the other hand, there is a rapid increase of the variogram with time until a time lag of approximately 4 days. Those features indicate that there is a varying ST dependence between the $PM_{2.5}$ concentrations in the domain defined by the 140 km, 4 days ranges. Only the $PM_{2.5}$ sampling points within these ranges around the (unsampled) point $\boldsymbol{p}_0$ are used to predict the corresponding $PM_{2.5}$ concentration at point $\boldsymbol{p}_0$ on the mapping grid. It is worth noting that, according to experience based on spatial interpolation, when the neighboring sampling points around the estimation (mapping grid) point $\boldsymbol{p}_0$ reach a certain number (e.g., 8 is usually sufficient), more sampling points at greater distances from $\boldsymbol{p}_0$ would have little influence on the estimated value and error variance (Webster and Oliver, 2007). This happens because the sampling points at greater distances will be assigned a very small weight λ, see Eq (3). In this study, for each space-time grid point there are enough monitoring sites within the (150 km, 4 days) ranges.

3.2. ST $PM_{2.5}$ predictions

The computational process leading to the generation of the ST $PM_{2.5}$ maps consisted of two stages: (*a*) STOK predictions of $PM_{2.5}$ concentrations at each point $\boldsymbol{p}_0$ on the mapping grid were derived using the $logPM_{2.5}$ data with the associated ST variogram model of Fig 3a; (*b*) subsequently, the $logPM_{2.5}$ values derived in the log-transformed domain were back-transformed (by means of anti-logarithms) to obtain the final $PM_{2.5}$ concentration maps in the original space-time domain (i.e., before log-transformation). These ST $PM_{2.5}$ maps are shown in Fig. 3b.

To test the prediction accuracy of the STOK technique, three standard accuracy indicators were computed based on the pairs of estimated-observed $PM_{2.5}$ concentrations of the validation set: the Pearson correlation coefficient (r), the mean error (ME), and the root mean squared error (RMSE). As shown in Fig. 4, the values of the r, ME and RMSE are 0.918, −0.89 $\mu g/m^3$ and 15.18 $\mu g/m^3$, respectively. The intercept and slope values of the regression line are 10.41 and 0.858, receptively. Since the value of slope are sufficiently close to 1, it is implied that in the validation set the estimated concentrations were very close to the observed $PM_{2.5}$ concentrations. Therefore, the three accuracy indicators of the STOK technique clearly demonstrate the high accuracy of the STOK technique in the mapping of $PM_{2.5}$ concentrations in the southern Jiangsu. Furthermore, based on the results obtained by the STOK technique and the relevant air pollution criterion described in Table 1 ($PM_{2.5}$>75 $\mu g/m^3$ indicates a polluted region of various levels), a meaningful description of ST $PM_{2.5}$ pollution in the southern Jiangsu was achieved. Lastly, Fig. S2 presents the polluted ST domain in southern Jiangsu. In fact, as will be shown in Fig. 6 later, about 29.3% of the ST domain was $PM_{2.5}$ polluted.

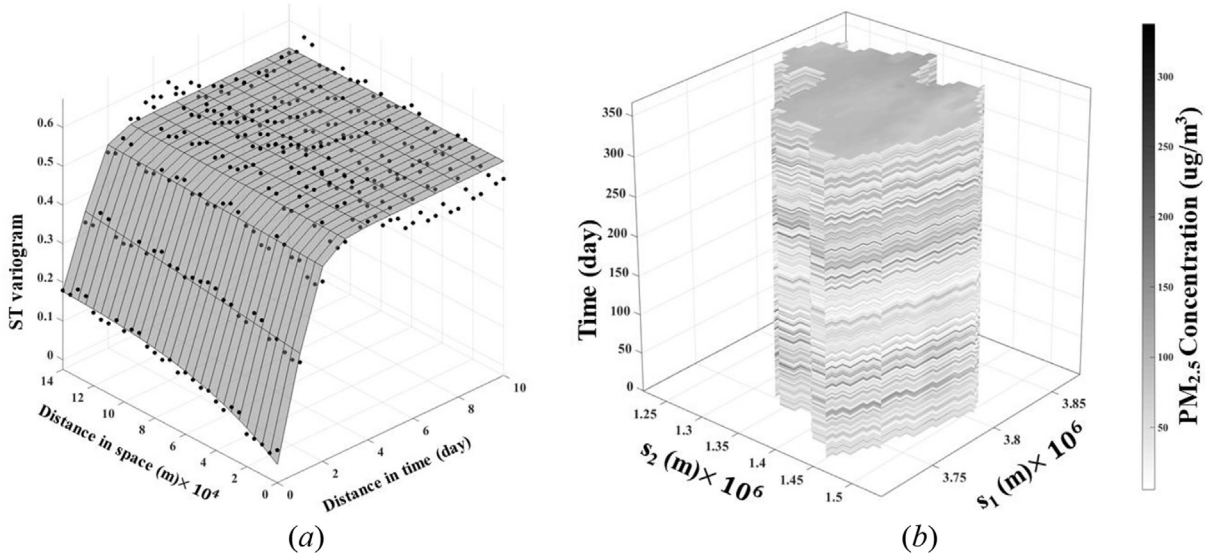

Fig. 3. (a) The empirical variogram values of log$PM_{2.5}$ concentrations (μg/m^3, black dots), and the theoretical variogram model (surface) fitted to these empirical values. (*b*) Plot of the ST map of predicted $PM_{2.5}$ concentration generated by the STOK technique.

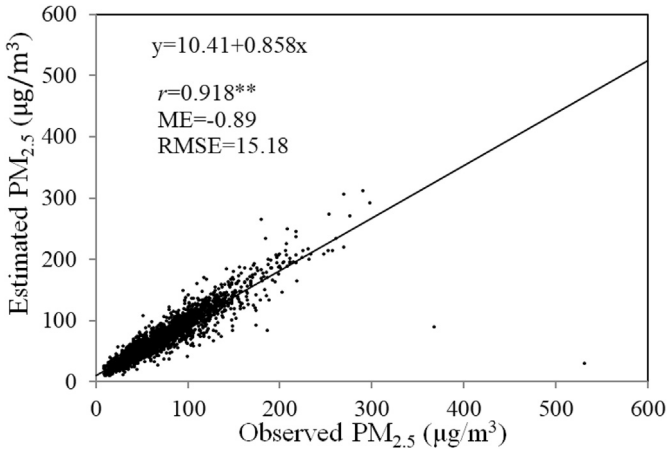

Fig. 4. Cross-validation results for the STOK technique.

3.3. ST querying and analysis

3.3.1. Spatial distribution of the $PM_{2.5}$ concentration mean and coefficient of variation (CV)

The given threshold value in Eq (6) is 75 μg/m^3. As is shown in Fig. 5a and b, the spatial distributions of $\overline{PM_{2.5}}(\boldsymbol{s})$ and $\overline{PM^{\geq}_{2.5}}(\boldsymbol{s})$, calculated by Eqs (5)–(6), were characterized by increasing concentration trends from east to west in the study region, indicating that meteorological factors had a significant effect on the $PM_{2.5}$ concentration levels, because the high wind speeds, relative humidity, abundant rainfall etc. of the eastern coastal areas create favorable conditions for the diffusion of $PM_{2.5}$ concentrations in the study region (Xu et al., 2017). Interestingly, as is shown in Fig. 5c and d, the spatial distribution of *CV*s exhibited similar patterns as the mean $PM_{2.5}$ concentrations.

3.3.2. Spatial distribution of the number of days exceeding the given threshold

As is shown in Fig. 6a–d, the number of days during 2014 with $PM_{2.5}$ concentrations exceeding the thresholds of 75, 115, 150, and 250 μg/m^3 varied from 59 to 164, 16 to 50, 1 to 22, and 0–3 days, respectively, in the entire study area. The plots in Fig. 6a–c showed a similar spatial pattern as the distribution of the annual mean $PM_{2.5}$ concentrations (Fig. 5a). This apparently happens because the higher the annual mean, the more days the $PM_{2.5}$ concentration exceeds the corresponding threshold. The number of days with $PM_{2.5}$ pollution (>75μg/m^3) were more than 151 in the western part of the study area, and it was heavily polluted (according to the classification of Table 1) during more than 18 of these days. Nanjing, the provincial capital of Jiangsu, experienced 3 days of serious pollution (see, Fig. 6d). On the other hand, as is clear in Fig. 6a–d, the eastern part of the study area experienced relatively good $PM_{2.5}$ air quality.

3.3.3. Temporal analysis of the $PM_{2.5}$ in different geographic locations

Fig S3 displays a three-dimensional (3D) plot of the mean $PM_{2.5}$ concentrations during every day of the year 2014 along the east-west direction of the study area. This plot reveals the considerable variability across space and in time. Perhaps more informative is the 3D plot of Fig. 7, which shows that in the time direction (day sequence), the $PM_{2.5}$ concentrations presented similar temporal pattern from the western to the eastern parts of the study area, which were characterized by 4 peaks and 3 troughs.

The interpretation of this pattern is as follows. The first and last peaks appeared during winter, and were caused by the local meteorological conditions, such as the high frequency of the inversion layer, lower rainfalls (most of the days during winter are cloudy, and only about 13% of days during winter are light rain), and human activities such as heating energy consumption. After the first peak, the $PM_{2.5}$ concentrations began to gradually decrease, affected by the strong winds during spring (see Fig. 8 (left)), the gradual increase of the surface temperature and the gradual enrichment of the vegetation (this is when the first trough occurs). Then, the rainy season arrived (called the plum rain season), and the accumulated pollutants in the region could not spread due to a subtropical high that resulted to hazy weather (the second peak). Next, during summer, the prevailing wind direction, mainly from an eastern marine air mass (see Fig. 8 (right)), with good cleaning performance and strong atmospheric wet deposition, contributed

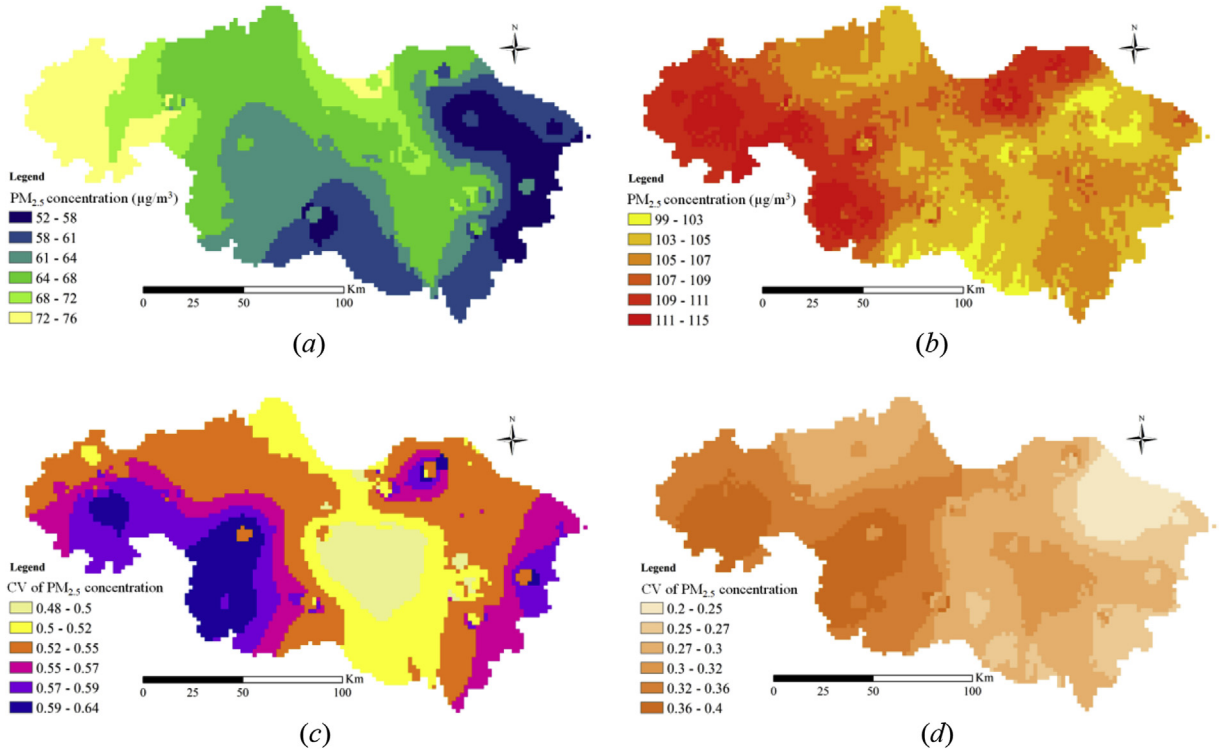

Fig. 5. (*a*) Spatial distribution of annual mean $PM_{2.5}$ concentrations ($\mu g/m^3$) and (*c*) corresponding *CV*. (*b*) Spatial distribution of the average $PM_{2.5}$ concentration during the days when the $PM_{2.5}$ concentration exceeded the threshold value and (*d*) corresponding *CV*.

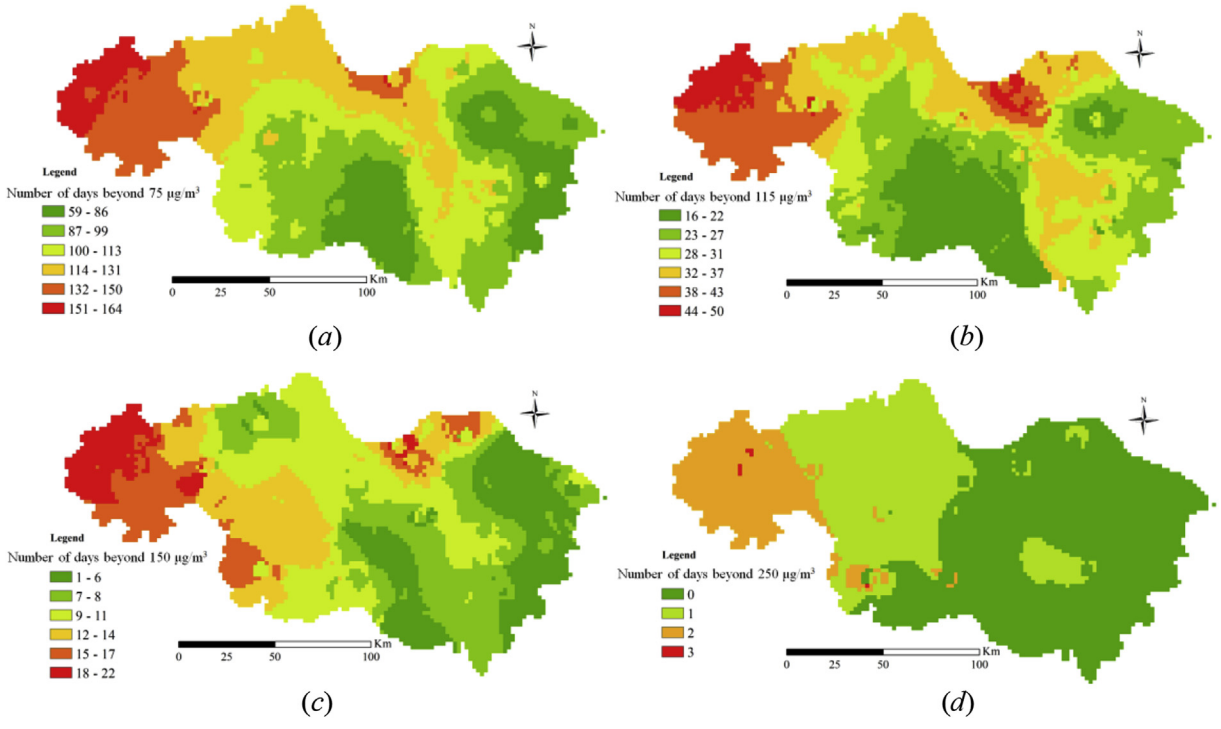

Fig. 6. Spatial distribution of the number of days of 2014 during which $PM_{2.5}$ concentrations exceeded (*a*) 75, (*b*) 115, (*c*) 150, and (*d*) 250 $\mu g/m^3$.

to the wet deposition and dilution of the air pollutants (the second trough). The autumn harvest season that followed was the peak period of straw burning, when a large amount of smoke was produced by open burning. Adverse meteorological conditions (small wind forces etc.; see Fig. 8 (left)) and the various pollutant sources have led to a $PM_{2.5}$ concentration increase in the area (the third peak). After the autumn harvest, the local pollution sources gradually decreased, resulting in a small $PM_{2.5}$ trough (the third one). In

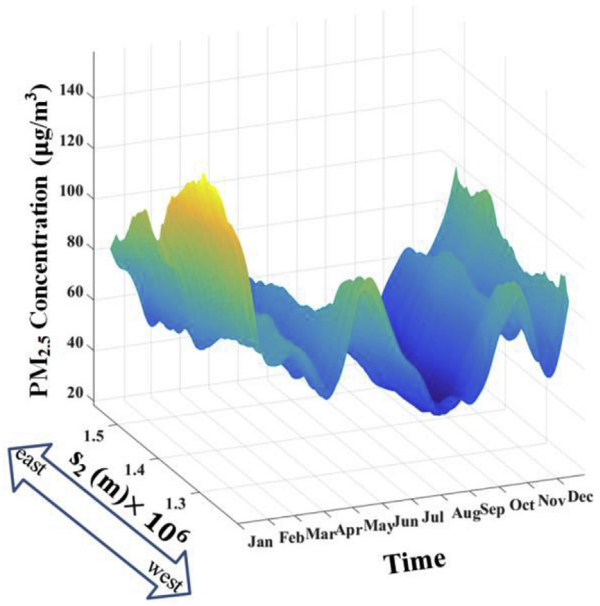

Fig. 7. Three-dimensional (3D) plot of the temporal trend for $PM_{2.5}$ concentrations during 2014 generated by the DHR method.

the S direction, from west to east, the mean $PM_{2.5}$ concentrations showed a significant decreasing trend (similar to that of Fig. 5a). The temporal variations of $PM_{2.5}$ concentrations observed in the study region were similar to relevant results of existing studies in other regions of China (Wang et al., 2014; Hu et al., 2014). And, some meteorological factors, including wind-force and temperature, were also identified to have a strong relationship with $PM_{2.5}$ variations (Huang et al., 2015). However, the results of the present study are based on a more detailed spatiotemporal analysis that integrated all the above factors and explicitly accounted for physical $PM_{2.5}$ correlations and dependencies, as a result of which the continuous ST distributions of $PM_{2.5}$ concentrations were obtained.

4. Conclusions and discussion

In this paper, the $PM_{2.5}$ concentration data of southern Jiangsu Province, China, collected during the year 2014, were used to compute an empirical $PM_{2.5}$ variogram characterizing the ST pollutant variation, and a theoretical model was found to have a close fit to the empirical variogram, which implied that the theoretical variogram model adequately characterized the actual ST $PM_{2.5}$ variation in the study area.

Subsequently, the theoretical variogram model served as the input to the STOK technique in order to generate predictions $PM^*_{2.5}(\boldsymbol{p}_0)$ of the $PM_{2.5}$ concentrations at unsampled ST points $\boldsymbol{p}_0$ on a mapping grid covering the study area during 2014. In addition to $PM^*_{2.5}(\boldsymbol{p}_0)$ at each $\boldsymbol{p}_0$, the uncertainty of the prediction was quantified by means of the prediction error variance $\sigma^2_{PM_{2.5}}(\boldsymbol{p}_0)$. The $PM^*_{2.5}(\boldsymbol{p}_0)$ maps are physical (real) maps, whereas the $\sigma^2_{PM_{2.5}}(\boldsymbol{p}_0)$ maps are conceptual maps that are valuable tools for risk assessment purposes. I.e., the values of the $PM^*_{2.5}(\boldsymbol{p}_0)$ maps can be physically measured in-situ (in the same way that the $PM_{2.5}$ data are), whereas the $\sigma^2_{PM_{2.5}}(\boldsymbol{p}_0)$ values cannot (yet, they offer valuable quantifications of our uncertainty concerning our $PM_{2.5}$ estimates). Three standard accuracy indicators were computed that demonstrated the high accuracy of the STOK maps of $PM_{2.5}$ distribution in the study area.

Lastly, ST analyses of the results obtained above (variogram plots and STOK maps) were used to describe the air pollution situation in the southern Jiangsu during 2014. The analysis showed that: (1) In 2014, about 29.3% of the area was polluted by $PM_{2.5}$ (at various levels of severity), according to the criteria established by the Chinese government, and the number of days characterized as polluted varied from 59 to 164 at different parts of the study area. Nanjing (the capital of Jiangsu province) was the place with the highest $PM_{2.5}$ pollution, including 3 days of serious pollution. (2) The $PM_{2.5}$ pollution showed a decreasing spatial trend from west to east in the study area; (3) The $PM_{2.5}$ concentrations showed a similar temporal distribution pattern from the western to the eastern part of southern Jiangsu that was characterized by 4 peaks and 3 troughs. The temporal variation was related to different meteorological and human factors.

Concluding, the STOK method was used in this study to establish a link between raw (monitoring) $PM_{2.5}$ data and a systematic ST pollutant analysis. This link implies, e.g., that higher STOK accuracy will result in more reliable $PM_{2.5}$ pollution assessment in the region. There are some factors, including the relative number of monitoring stations (i.e., the ratio of the number of monitoring stations over the area of the study region), auxiliary information and the preliminary ST trend analysis and modeling preceding STOK implementation, which can affect STOK accuracy. Obviously, more monitoring stations will improve STOK accuracy, because the computation of the ST variogram used by STOK becomes more accurate and realistic with an increasing number of sampling

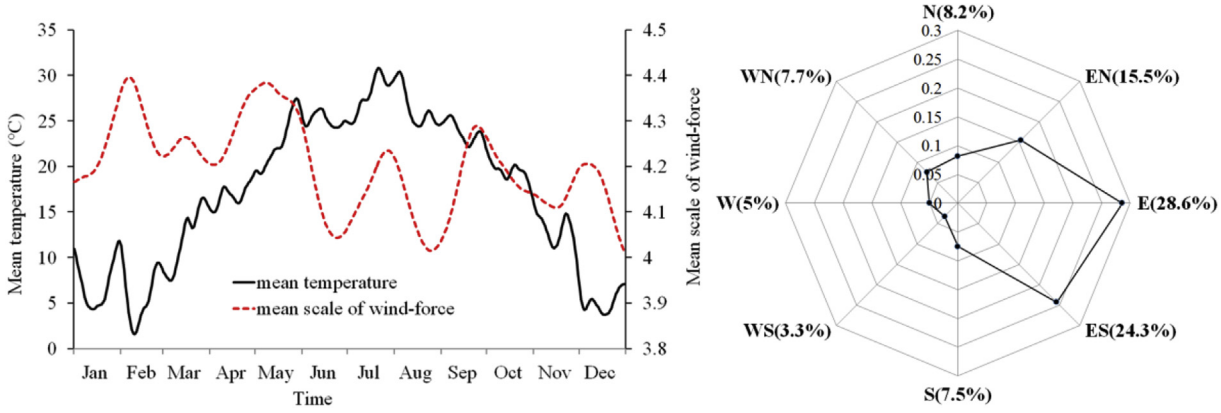

Fig. 8. Plot of the mean temperature and mean scale of wind-force along with day sequence (left), and rose plot of wind direction in the summer of 2014 (right). The temperature, wind-force and wind direction data were collected from the Jiangsu Meteorological Bureau. The daily data were recorded for each city. The daily "wind-force" data were calculated by averaging "wind-force" values from the five cities.

points. Furthermore, as the number of stations increases, more neighboring sampling points that are closer to the $PM_{2.5}$ prediction points will be involved in the solution of the STOK system of Eq (2), leading to smaller prediction error variances calculated by Eq (4). If the number of monitoring stations is fixed, the use of auxiliary information from various sources can improve $PM_{2.5}$ prediction accuracy across space-time.

As regards these auxiliary information sources, recent studies have found that in several regions of the world the aerosol optical depth (AOD) data obtained from satellite measurements (such as the Moderate Resolution Imaging Spectroradiometer, MODIS, and the Multiangle Imaging SpectroRadiometer, MISR) are correlated with $PM_{2.5}$ concentrations (Zhang et al., 2009; Hutchison et al., 2005). Furthermore, other studies have used AOD data to predict the ST variations of $PM_{2.5}$ concentrations (You et al., 2015; Yang et al., 2007). However, the correlation between AOD and $PM_{2.5}$ varied with the change of season and between different regions resulting in lower $PM_{2.5}$ prediction accuracy in some regions and time periods. Therefore, it is worth of further study the way data from monitoring stations can be combined with AOD data to improve the ST prediction accuracy of $PM_{2.5}$ pollution assessment.

The varying $PM_{2.5}$ trend in the southern Jiangsu region during the specified period generated by the DHR technique (Fig. 7) can be physically explained by geographical location, varying distances from emission sources (vehicle emissions, power plants, coal combustion, smelting industry, steel industry and minerals), and meteorological factors (e.g., temperature, force and direction of wind discussed in section 3.3.3).

Generally, trend determination in a map is affected by one's understanding of the phenomenon, observation scale, study objectives, contextual details and perceived scale, and is not a purely statistical matter. In this context, an apparent limitation of the present analysis is that the STOK was directly implemented to generate $PM_{2.5}$ concentration maps, without a preliminary ST trend modeling (i.e., preceding the STOK implementation). The technical and methodological reasons for this modeling choice included the following:

(1) *Insufficient data*: That is, the study-specific difficulties of a realistic and rigorous modeling of the spatial trend. Specifically, (1*a*) it is very hard to fit a realistic ST $PM_{2.5}$ trend model in terms of ST position data alone, without sufficient auxiliary data (source apportionment was not possible because the necessary detailed data, e.g., about the chemical $PM_{2.5}$ characteristics, were not available for the year 2014), and (1*b*) an inadequate ST trend model will not lead to improved ST prediction accuracy. In order to test assertions (1*a*) and (1*b*) numerically, the STOK with trend model (STKT) was employed to predict ST distribution of $PM_{2.5}$ concentrations using the same training data set and validation data set in the Supplemental Materials II. The STKT results showed that assertions (1*a*) and (1*b*) above are, indeed, valid in the present case study.

(2) *Methodological perspective*: In the present case study, the original $PM_{2.5}$ data (involving a trend) were logarithmically transformed, and the variogram of the data in the new space-time domain (Fig. 3a) clearly indicated a transformed $PM_{2.5}$ dataset that is not characterized by significant trends (e.g., the variogram has a definite sill along the space-time lags, whereas a dataset with trends should lead to a variogram with no sill). So, using STOK on the transformed dataset was deemed appropriate. Of course, the STOK results were finally back-transformed into the original ST domain, which restored the ST trend in the back-transformed $PM_{2.5}$ estimates, as shown in the figures with the $PM_{2.5}$ maps.

(3) *Computational issues*: In our previous study (Yang et al., 2015), the ST trend was inserted into the prediction model using soil heavy metal Cd values as experimental data. The results showed that adequate trend modeling can improve ST prediction accuracy. The difference is that while in that study the soil Cd had a simple variation pattern across space and time, in the present study the variation patterns of $PM_{2.5}$ across space and time are much more complex and the datasets very large (note that the number of monitoring data is over 15000), resulting to serious computational difficulties.

Lastly, it should be noticed that when sufficient information concerning apportionment sources becomes available, it should be worth investigating how this important information can improve the current $PM_{2.5}$ analysis and modeling.

Acknowledgements

This research was supported by the National Key R&D Program of China (Grant No. 2017YFA0605002), the National Natural Science Foundation of China (Grants No. 41671217 and 41671399), and a project supported by the Fundamental Research Funds for the Central Universities (Grant No. 2662017PY038).

Appendix A. Supplementary data

Supplementary data related to this article can be found at https://doi.org/10.1016/j.envpol.2017.11.077.

References

Calculli, C., Fassò, A., Finazzi, F., Pollice, A., Turnone, A., 2015. Maximum likelihood estimation of the multivariate hidden dynamic geostatistical model with application to air quality in Apulia, Italy. Environmetrics 26, 406–417. https://doi.org/10.1002/env.2345.

Chen, T., He, J., Lu, X., She, J., Guang, Z., 2016. Spatial and temporal variations of $PM_{2.5}$ and its relation to meteorological factors in the urban area of Nanjing, China. Int. J. Environ. Res. Public Health 13, 921.

Christakos, G., 1992. Random Field Models in Earth Sciences. Academic Press, San Diego, CA. New Edition (2005), Dover Publ. Inc., Mineola, NY.

Christakos, G., 2017. Spatiotemporal Random Fields: Theory and Applications, second ed. Elsevier, Cambridge, MA.

Christakos, G., Hristopulos, D.T., 1998. Spatiotemporal Environmental Health Modelling: a Tractatus Stochasticus. Kluwer Academic Publ., Boston, MA.

Christakos, G., Serre, M.L., 2000. BME analysis of spatiotemporal particulate matter distributions in North Carolina. Atmos. Environ. 34, 3393–3406. https://doi.org/10.1016/S1352-2310(00)00080-7.

Christakos, G., Serre, M.L., Kovitz, J., 2001. BME representation of particulate matter distributions in the state of California on the basis of uncertain measurements. J. Geophys. Res. Atmos. 106, 9717–9731.

Datta, A., Banerjee, S., Finley, A.O., Hamm, N.A.S., Schaap, M., 2016. Nonseparable dynamic nearest neighbor Gaussian process models for large spatio-temporal data with an application to particulate matter analysis. Ann. Appl. Stat. 10, 1286–1316. https://doi.org/10.1214/16-AOAS931.

De Iaco, S., Myers, D.E., Posa, D., 2003. The Linear Coregionalization model and the product-sum space-time variogram. Math. Geol. 35, 25–38. https://doi.org/10.1023/A:1022425111459.

De Cesare, L., Myers, D.E., Pose, D., 2001. Product-sum covariance for space-time modeling: an environmental application. Environmetrics 12, 11–23. https://doi.org/10.1002/1099-095X(200102)12:1%3c11::AID-ENV426%3e3.3.CO;2-G.

Fang, C., Wang, Z., Xu, G., 2016. Spatial-temporal characteristics of $PM_{2.5}$ in China: a city-level perspective analysis. J. Geogr. Sci. 26, 1519–1532. https://doi.org/10.1007/s11442-016-1341-9.

Fassò, A., Finazzi, F., Ndongo, F., 2016. European population exposure to airborne pollutants based on a multivariate spatio-temporal model. J. Agric. Biol. Environ. Stat. 21, 492–511. https://doi.org/10.1007/s13253-016-0260-7.

Gneiting, T., 2002. Nonseparable, stationary covariance functions for space–time data. J. Am. Stat. Assoc. 97, 590–600. https://doi.org/10.1198/016214502760047113.

Hu, J.L., Wang, Y.G., Ying, Q., Zhang, H.L., 2014. Spatial and temporal variability of PM2.5 and PM10 over the north China plain and the yangtze river delta, China. Atmos. Environ. 95, 598–609. https://doi.org/10.1016/j.atmosenv.2014.07.019.

Hutchison, K.D., Smith, S., Faruqui, S.J., 2005. Correlating MODIS aerosol optical thickness data with ground-based $PM_{2.5}$ observations across Texas for use in a

real-time air quality prediction system. Atmos. Environ. 39, 7190–7203. http://doi:10.1016/j.atmosenv.2005.08.036.
Huang, F., Li, X., Wang, C., Xu, Q., Wang, W., Luo, Y., Tao, L., Gao, Q., Chen, S., Cao, K., Liu, L., Gao, N., Liu, X., Yang, K., Yan, A., Guo, X., 2015. $PM_{2.5}$ spatiotemporal variations and the relationship with meteorological factors during 2013-1014 in Beijing, China. PLoS One 10, e0141642. http://doi:10.1371/journal.pone.0141642.
Jiang, B., Liang, S.L., Wang, J.D., Xiao, Z.Q., 2010. Analysis and prediction of MODIS LAI time series with Dynamic Harmonic Regression model. J. Remote Sens. 14, 13–32.
Kolovos, A., Christakos, G., Hristopulos, D.T., Serre, M.L., 2004. Methods for generating non-separable spatiotemporal covariance models with potential environmental applications. Adv. Water Resour. 27, 815–830. https://doi.org/10.1016/j.advwatres.2004.04.002.
Ma, C., 2008. Recent developments on the construction of spatio-temporal covariance models. Stoch. Environ. Res. Risk Assess. 22, S39–S47. https://doi.org/10.1007/s00477-007-0154-x.
Ministry of Environmental Protection of the People's Republic of China (MEPPRC), 2012. China National Ambient Air quality Standards. Available at: http://kjs.mep.gov.cn/hjbhbz/bzwb/dqhjbh/dqhjzlbz/201203/W020120410330232398521.pdf.
National Health & Family Planning Commission of China (NHFPCC), 2013. Chinese Health and Family Planning Statistical Yearbook for 2013. China, Beijing.
Pang, W., Christakos, G., Wang, J.F., 2009. Comparative spatiotemporal analysis of fine Particulate Matter pollution. Environmetrics 21, 305–317. https://doi.org/10.1002/env.1007.
Porcu, E., Mateu, J., Saura, F., 2008. New classes of covariance and spectral density functions for spatio-temporal modelling. Stoch. Environ. Res. Risk Assess. 22, S65–S79. https://doi.org/10.1007/s00477-007-0160-z.
Shen, G.F., Yuan, S.Y., Xie, Y.N., Xia, S.J., Li, L., Yao, Y.K., Qiao, Y.Z., Zhang, J., Zhao, Q.Y., Ding, A.J., 2014. Ambient levels and temporal variations of PM2.5 and PM10 at a residential site in the mega-city Nanjing, in the western Yangtze River Delta, China. J. Environ. Sci. Health Part A-Toxic/Hazardous Subst. Environ. Eng. 49, 171–178. https://doi.org/10.1080/10934529.2013.838851.
Snepvangers, J.J.J.C., Heuvelink, G.B.M., Huisman, J.A., 2003. Soil water content interpolation using spatio-temporal kriging with external drift. Geoderma 112, 253–271. https://doi.org/10.1016/S0016-7061(02) 00310–00315.
Wang, F., Meng, D., Li, X.W., Tan, J.J., 2016. Indoor-outdoor relationships of PM2.5 in four residential dwellings in winter in the Yangtze River Delta, China. Environ. Pollut. 215, 280–289. https://doi.org/10.1016/j.envpol.2016.05.023.
Wang, Y., Ying, Q., Hu, J., Zhang, H., 2014. Spatial and temporal variations of six criteria air pollutants in 31 provincial capital cities in China during 2013-2014. Environ. Int. 73, 413–422. https://doi.org/10.1016/j.envint.2014.08.016.
Wang, Z.B., Fang, C.L., 2016. Spatial-temporal characteristics and determinants of $PM_{2.5}$ in the bohai rim urban agglomeration. Chemosphere 148, 148–162. https://doi.org/10.1016/j.chemosphere.2015.12.118.
Webster, R., Oliver, M.A., 2007. Geostatistics for Environmental Scientists, second ed. John & Wiley & Sons, Ltd, Chichester (England), pp. 172–173.
Xu, J., Kuang, H., Wang, G., Chen, M., Lu, L., 2017. Analysis of the relationship between PM2.5 and relative humidity in air. Agric. Technol. 37 (148–149), 157 (in Chinese).
Yang, L., Franklin, M., Kahn, R., Koutrakis, P., 2007. Using aerosol optical thickness to predict ground-level $PM_{2.5}$ concentrations in the St. Louis area: a comparison between MISR and MODIS. Remote Sens. Environ. 107, 33–44. https://doi.org/10.1016/j.rse.2006.05.022.
Yang, Y., Mei, Y., Zhang, C., Zhang, R., Liao, X., 2014. Spatio-temporal modeling and prediction of soil heavy metal based on spatio-temporal Kriging. Trans. Chin. Soc. Agric. Eng. 30, 249–255 (in Chinese with English abstract).
Yang, Y., Wu, J., Christakos, G., 2015. Prediction of soil heavy metal distribution using spatiotemporal Kriging with trend model. Ecol. Indic. 56, 125–133. https://doi.org/10.1016/j.ecolind.2015.03.034.
You, W., Zang, Z., Pan, X., Zhang, L., Chen, D., 2015. Estimating PM2.5 in Xi'an, China using aerosol optical depth: a comparison between the MODIS and MISR retrieval models. Sci. Total Environ. 505, 1156–1165. https://doi.org/10.1016/j.scitotenv.2014.11.024.
Young, P.C., Pedregal, D.J., Tych, W., 1999. Dynamic harmonic regression. J. Forecast. 18, 369–394.
Young, P.C., Taylor, C.J., Tych, W., Pedregal, D.J., 2007. The Captian Toolbox. Centre for Research on Environmental Systems and Statistics. Lancaster University, UK. Internet. www.es.lancs.ac.uk/cres/captain.
Zhang, H., Hoff, R.M., Engle-Cox, J.A., 2009. The relation between moderate resolution imaging spectroradiometer (MODIS) aerosol optical depth and $PM_{2.5}$ over the United States: a geographical comparison by U.S. Environmental Protection Agency Regions. J. Air & Waste Manag. Assoc. 59, 1385–1369. https://doi.org/10.3155/1047-3289.59.11.1358.
Zhang, Z.H., Hu, M., Ren, J., Zhang, Z.Y., Christakos, G., Wang, J.F., 2017. Probability assessment of particulate matter (PM10) in beijing, China. Atmos. Pollut. Res. https://doi.org/10.1016/j.apr.2017.04.006.
Zhao, C.X., Wang, Y.Q., Wang, Y.J., Zhang, H.L., Zhao, B.Q., 2014. Temporal and spatial distribution of PM2.5 and PM10 pollution status and the correlation of particulate matters and meteorological factors during winter and spring in Beijing. Environ. Sci. 35, 418–427 (in Chinese with English abstract).